Supporting Information

Smith et al. 10.1073/pnas.1218173110

SI Materials and Methods

Plasmid Constructs and Antibodies. Human cDNA encoding wild-type H-RAS (Gene ID: 3265, residues 1–171), or the oncogenic mutants G12V/Q61L/G13D were cloned into pET15b (Novagen/EMD Biosciences) for bacterial expression with an N-terminal polyhistidine (His) tag. The GAP-334 region from human p120GAP (Gene ID: 5921, residues 715–1047) and the SOS^{cat} domain from human SOS1 (Gene ID: 6654, residues 564–1049) were also subcloned and expressed in pET15b. A construct expressing the BRAF RAS binding domain (RBD) (Gene ID: 673, residues 150–233) with N-terminal GST tag was subcloned from human cDNA into pGEX-4T2 (Amersham Pharmacia Biotech). $BRAF^{GDP}$ mutations A184K and P170R were generated and expressed in the pGEX-4T2 vector. For mammalian expression of wild-type and GDP-binding BRAF RBDs, cDNA were subcloned into the pEGFP-C1 (Clontech) backbone, with N-terminal dsRed tag fused in place of EGFP. For expression of full-length p120GAP and SOS1 for NMR analysis, cDNAs were cloned and expressed from the pcDNA5/FRT/TO plasmid as part of the Flp-In T-Rex system (Invitrogen) for generating stable, Tet-inducible expression lines. SOS1 mutants, including the HF (E108K), DH (E268A/M269A/D271A), PH-Rem linker (R552G), allosteric (W729E), and Noonan Syndrome (NS) (T37A, K170E, I252T, Y337C, G434R, C441Y, S548R, L550P, P655L, Y702H, I733F, P894R, Q977R) were generated in pcDNA5/FRT/TO. All constructs were sequence-verified.

The anti-Flag M2 and anti-tubulin MAbs was purchased from Sigma. Rabbit polyclonal anti-ERK and anti-RAS antibodies were from Millipore, anti-RFP from Chemicon International, anti-pERK from Cell Signaling Technology, anti-NF1, anti-GAPDH, and anti-p120GAP from Santa Cruz.

Purification of Recombinant Proteins. GST or His-tagged proteins were expressed in *Escherichia coli* BL21 cells grown in minimal M9 or LB media by induction with isopropyl-b-D-thiogalactopyranoside at 15 °C overnight. Generally, cells were lysed and sonicated in 20 mM Tris (pH 7.5), 150 mM NaCl, 10% (vol/vol) glycerol, 0.4% Nonidet P-40, protease inhibitors (Roche), 1 mM phenylmethylsulfonyl fluoride (PMSF), 10 ng/mL^{-1} DNase, and either 1 mM DTT or 10 mM β-mercaptoethanol. Lysate was cleared by centrifugation and incubated with glutathione (Amersham Pharmacia Biotech) or Ni-NTA (Qiagen) resin at 4 °C for 2 h. Bound proteins were eluted directly with thrombin cleavage or with 250 mM imidazole (Bioshop) followed by thrombin. Concentrated proteins were purified to homogeneity by size exclusion chromatography using either an S75 or S200 column (GE Healthcare). Recombinant wild-type RAS is purified from *E. coli* predominantly in the GDP-bound form; oncogenic variants are regularly bound to GTP. These proteins were preloaded with GMPPNP, GTP, GDP, or GTPγS (Sigma) when required. For NMR-based GAP assays, aliquots of RAS-GTP could be flash-frozen at a precise time point in the hydrolysis reaction and stored at −80 °C with no perceptible change in activity.

Cell Culture, RBD Pull Downs, and Western Blotting. Human HEK 293 and CRL-2884, rat CRL-2769 cells were maintained in DMEM containing 10% (vol/vol) FCS and antibiotics. CRL-2769 and CRL-2884 were purchased from ATCC. For exogenous expression, cells were transiently transfected with PEI. Full-length p120GAP stable cell lines were derived using the Flp-In T-Rex protocol (Invitrogen). Tet-induction was done with 2 μg/mL over 48 h. EGF (PeproTech) or media containing 10% (vol/vol) serum were added after culturing overnight in the absence of serum at indicated times and concentrations. Phase images were taken on a Leica DMIRE2 inverted microscope (Quorum Technologies).

For cell-based SOS1 assays and characterization of Schwann control and malignant peripheral nerve sheath tumor-derived lines, cells were lysed in TXNP buffer [20 mM Tris (pH 7.5), 150 mM NaCl, 10% (vol/vol) glycerol, 1% Triton X-100, 1% Nonidet P-40, 1 mM DTT, 5 mM $MgCl_2$, 1 mM sodium vanadate, 1 mM PMSF, and protease inhibitors] and lysates cleared by centrifugation. A fraction of each lysate were separated by SDS/PAGE and transferred to a nitrocellulose membrane (Schleicher and Schuell Bioscience). Remaining lysates were used for determining RAS-GTP levels, performed immediately with glutathione beads carrying recombinant GST-BRAF RBD. Equal amounts of beads were added to SOS1 lysates and incubated for 15 min at 4 °C, followed by washing five times with TXNP buffer, separation by SDS/PAGE and transfer to a nitrocellulose membrane. For the BRAF wild-type/GDP mutant binding experiment, His-tagged RAS proteins bound to nickel beads were preloaded with GDP or GMPPNP and incubated with lysates containing recombinant RFP-BRAF RBD domains for 15 min at 4 °C in TXNP buffer (plus 10 mM β-mercaptoethanol and 30 mM imidazole). Bound proteins were washed five times with TXNP buffer, separated by SDS/PAGE, and transferred to a nitrocellulose membrane. All membranes were blocked in TBST containing 5% (wt/vol) skim milk and immunoblotted. Primary antibodies were detected with anti-mouse Ig or anti-rabbit Ig antibodies conjugated to horseradish peroxidase followed by treatment with ECL (Pierce).

NMR Spectroscopy. All NMR data were recorded at 25 °C on an 800 MHz Bruker AVANCE II spectrometer equipped with a 5 mm TCI CryoProbe, or a 600 MHz Bruker UltraShield spectrometer with 1.7 mm CryoProbe. Two-dimensional $^{1}H/^{15}N$ heteronuclear single quantum coherence (HSQC) (1) spectra as well as triple resonance HNCACB, CBCACONH, and HNCA spectra were collected for the backbone chemical-shift assignments. All NMR samples were prepared in buffer containing 20 mM Tris (pH 7.5), 100 mM NaCl, 1 mM DTT, 5 mM $MgCl_2$, and 10% (vol/vol) D_2O. Spectra were processed with NMRPipe (2) and resonance assignments made with NMRView (3).

Membrane Fractionation. Transfected cells were resuspended in homogenization buffer [0.25 M sucrose, 78 mM KCl, 4 mM $MgCl_2$, 8.4 mM $CaCl_2$, 10 mM EGTA, protease inhibitors, 50 mM Hepes-NaOH (pH 7.0)] and homogenized using repeated passage through a 27-G syringe. The homogenate was cleared by centrifugation at $1,000 \times g$ for 10 min, and supernatant fractionated by centrifugation at $100,000 \times g$ for 30 min in an Airfuge (Beckman). Supernatant (cytosol) and pellet (membrane) were separated by SDS/PAGE and analyzed by immunoblotting.

Statistical Analysis. One-way ANOVA tests ($P < 0.0001$) were used to analyze groups of densitometry or NMR data, followed by Bonferroni's Multiple Comparison Test. For direct comparison of two datasets, two-tailed unpaired t tests ($P < 0.05$) were used.

1. Bodenhausen G, Ruben D (1980) Natural abundance 15N NMR by enhanced heteronuclear spectroscopy. *Chem Phys Lett* 69:185–189.
2. Delaglio F, et al. (1995) NMRPipe: A multidimensional spectral processing system based on UNIX pipes. *J Biomol NMR* 6(3):277–293.
3. Johnson BA (2004) Using NMRView to visualize and analyze the NMR spectra of macromolecules. *Methods Mol Biol* 278:313–352.

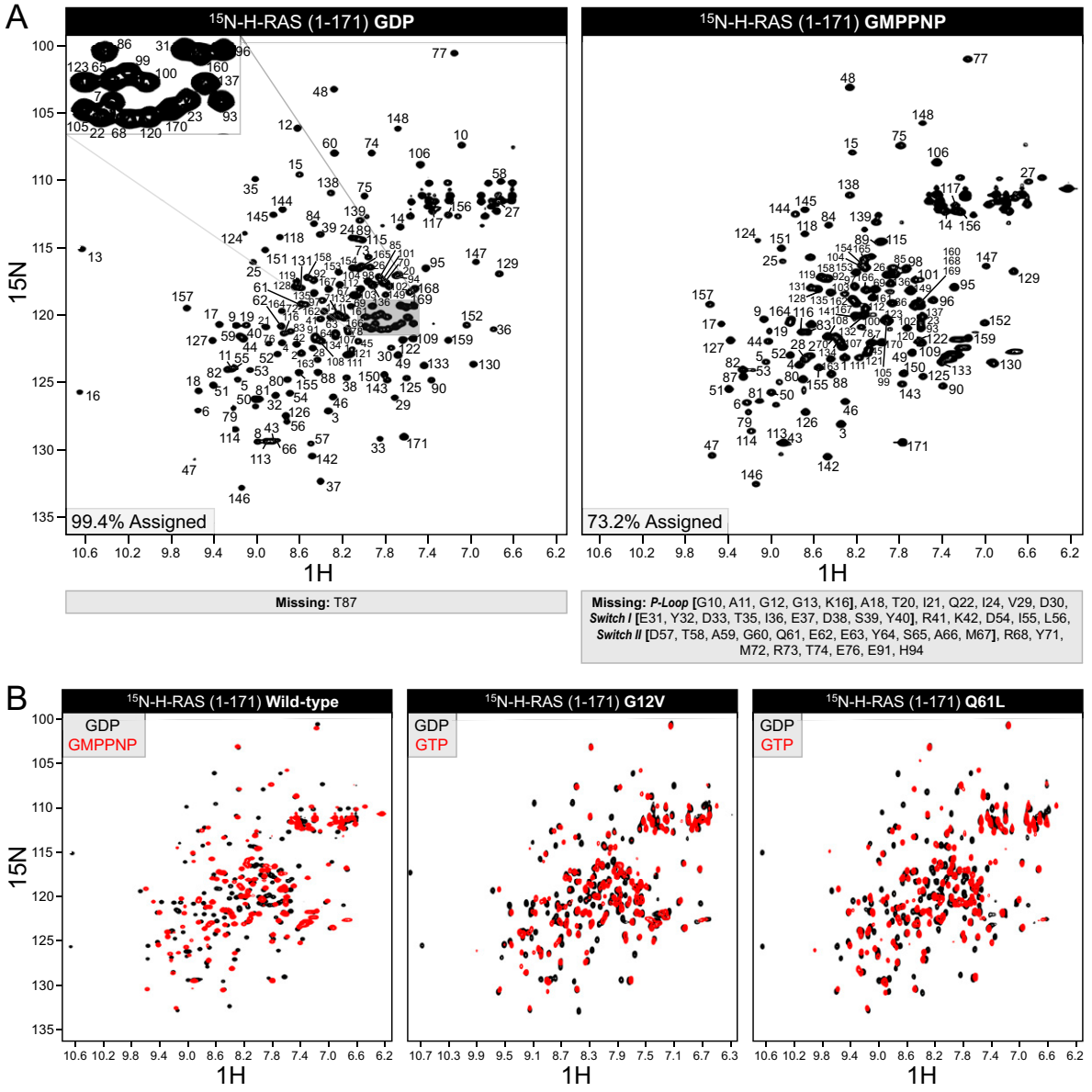

Fig. S1. Assignment of H-RAS backbone and discrepancies in HSQC spectra dependent on nucleotide-bound state. (*A*) Backbone amide resonances were assigned for RAS (residues 1–171) bound to GDP or GMPPNP. (*Left*) Two-dimensional $^{1}H/^{15}N$ HSQC of RAS in the GDP-bound state; 99.4% of backbone amide resonances were assigned using standard triple resonance experiments (HNCACB, CBCACONH) on $^{15}N/^{13}C$ protein. (*Right*) Next, 73.2% of backbone resonances were assigned after exchange with GMPPNP. Missing resonances are mostly confined to the P-loop and Switch regions (listed at the bottom). (*B*) HSQC overlays of wild-type or oncogenic mutants of RAS show deviations generated by differential nucleotide binding. Here, wild-type RAS (*Left*) is bound to GDP (black) or GMPPNP (red) as above. The RAS mutants G12V (*Center*) and Q61L (*Right*) are bound to GDP (black) or unmodified GTP (red).

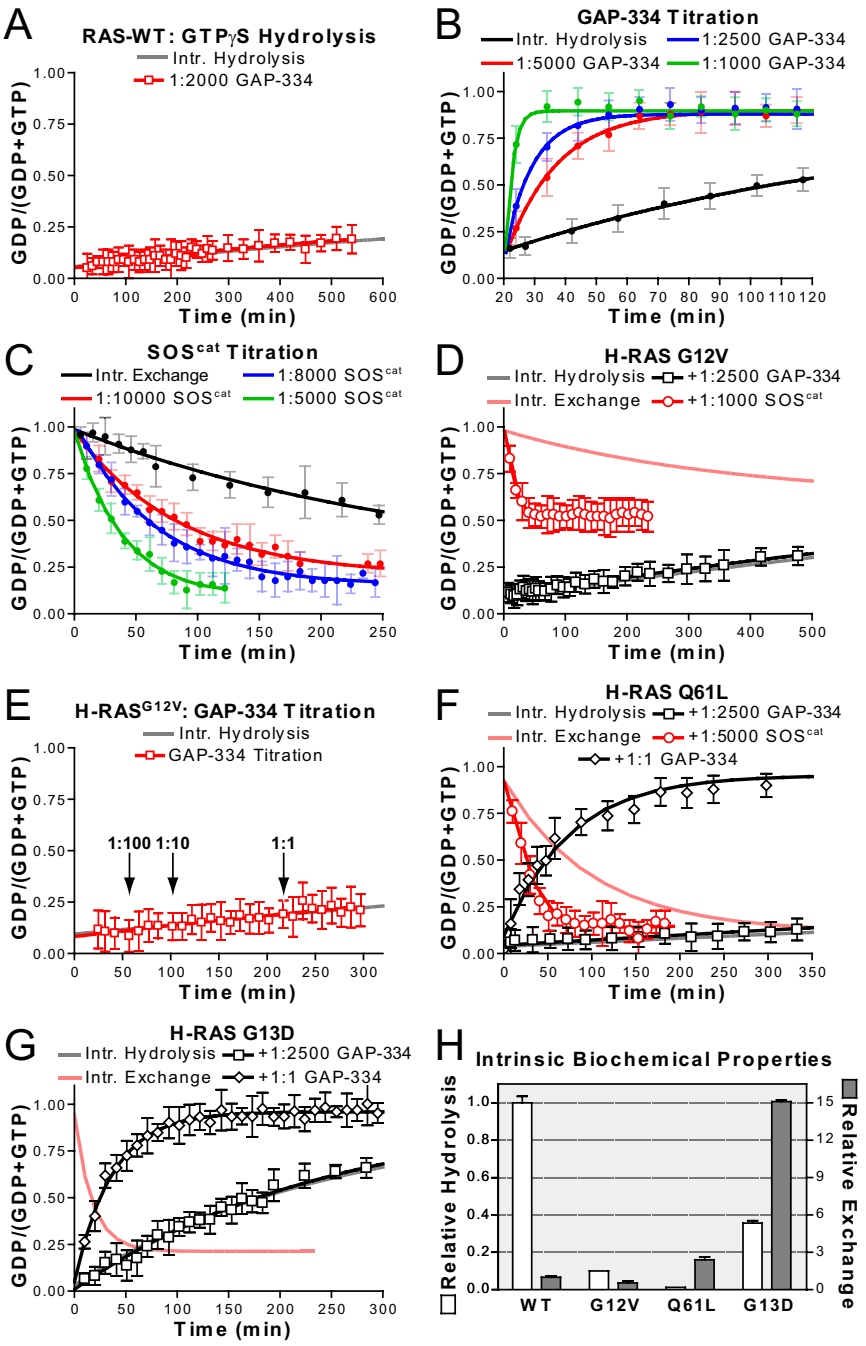

Fig. S2. NMR-derived hydrolysis and exchange activities. (*A*) Hydrolysis of the GTPγS analog by wild-type RAS. The rate of GTPγS hydrolysis is extremely slow and does not affect calculated exchange rates. Addition of GAP-334 is not capable of stimulating GTPγS hydrolysis. (*B*) Capacity of GAP-334 to stimulate GTPase activity can be measured through sequential dilution (i.e., lowering the ratio of GAP-334-to-RAS). (*C*) SOS^{cat} stimulation of RAS nucleotide exchange can also be monitored with lower ratios of SOS^{cat}-to-RAS, here in the presence of 10-fold molar excess GTPγS. (*D*) Properties of the RAS oncogenic mutant G12V. Slow intrinsic exchange is stimulated 55-fold by 1:1,000 SOS^{cat}, GAP-334 had no capacity to stimulate hydrolysis. (*E*) Equimolar concentration of GAP-334 is still unable to stimulate GTP hydrolysis of the RAS oncogenic mutant G12V. ^{15}N-RAS^{G12V} was preloaded with GTP and hydrolysis monitored by NMR. Addition of 1:100, 1:10, or 1:1 molar ratios of GAP-334 did not stimulate the slow intrinsic GTP hydrolysis rate. (*F*) Hydrolysis and exchange of the RAS oncogenic mutant Q61L. Fast intrinsic exchange is increased 5-fold by 1:5,000 SOS^{cat}, addition of 1:2,500 GAP-334 does not affect GTP hydrolysis. GAP-334 at 1:1 does stimulate Q61L GTP hydrolysis (148×). (*G*) Properties of RAS oncogenic mutant G13D. 1:2,500 GAP-334 did not stimulate hydrolysis, but equimolar concentrations of GAP-334 increased the hydrolysis rate 9 fold. Extremely rapid intrinsic exchange precluded measurements of GEF-mediated activation. (*H*) Summary of the intrinsic biochemical properties of wild-type RAS and the oncogenic mutants G12V, Q61L, and G13D. Hydrolysis (left axis) and exchange (right axis) rates are shown relative to wild-type RAS.

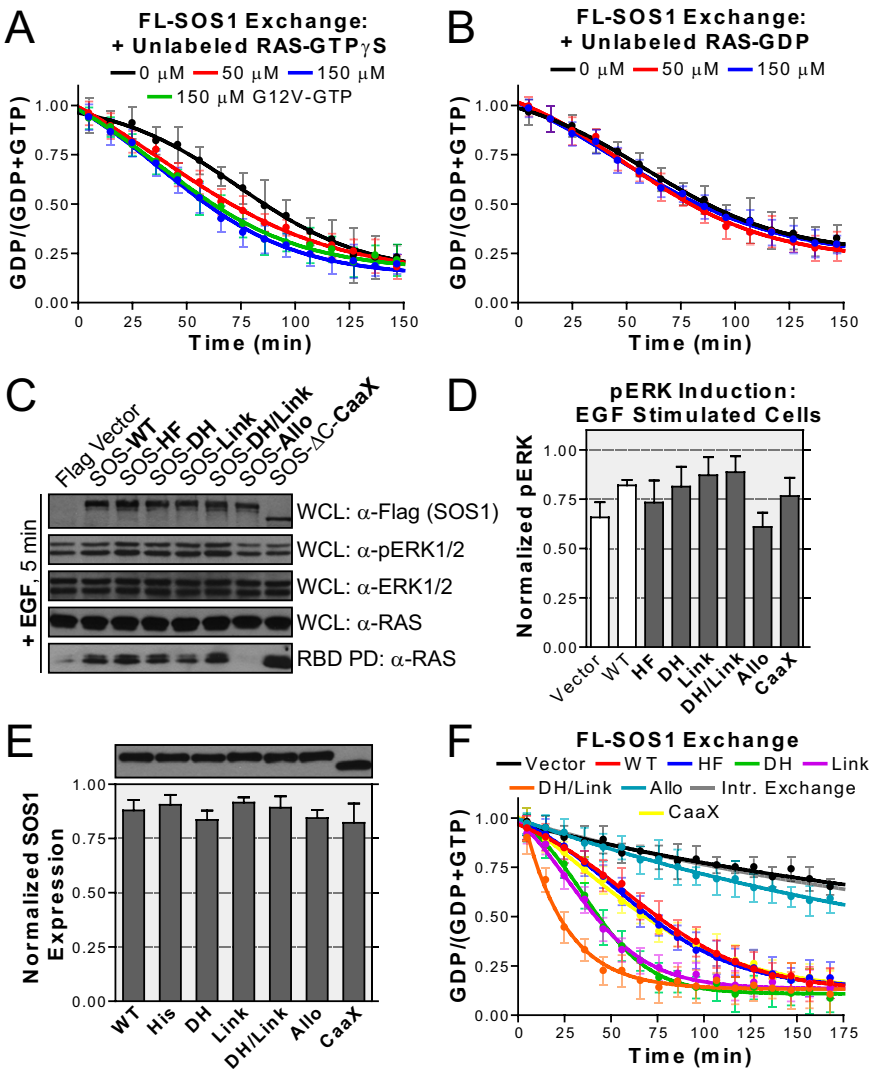

Fig. S3. Cell-based assays and NMR-derived data reveal the effect of mutations on regulation and activity of full-length SOS1. (*A*) Addition of activated RAS stimulates full-length SOS1 activity, restoring an exponential fit. Unlabeled, wild-type RAS exchanged with GTPγS or RAS^{G12V} exchanged with GTP were mixed with ^{15}N-RAS-GDP at indicated concentrations before addition of wild-type SOS1 lysates. (*B*) Increasing RAS concentration by addition of excess RAS-GDP does not stimulate SOS1 activity, and retains a sigmoidal fit (compare with plot in *A*). Unlabeled, wild-type RAS bound to GDP was mixed with ^{15}N-RAS-GDP and 10-fold molar excess GTPγS at indicated concentrations before addition of lysate containing wild-type SOS1. (*C*) SOS1 mutants activate the RAS/RAF/MAPK pathway when expressed in cells. Full-length wild-type and mutant (see Fig. S4) SOS1 proteins were Flag-tagged and expressed in HEK 293T cells. Membrane-targeted SOS1-ΔC-CaaX was included as a positive control. Western blots showing expressed SOS1 levels (anti-Flag), activated ERK (anti-pERK), loaded ERK (anti-ERK), loaded RAS (anti-RAS), and activated RAS (GST-BRAF RBD pull-down, anti-RAS) are shown for EGF-stimulated cells. Analogous blots for starved cells are presented in Fig. 4*B*. Results are representative of multiple repeated experiments. (*D*) Quantitation of ERK activation in cells expressing wild-type or mutant SOS after stimulation with EGF for 5 min. Data are derived from densitometry analysis of Western blots from three separate experiments. One-way ANOVA detects no significant difference in mean pERK levels. (*E*) Quantitation of Flag-SOS1 expression as determined from densitometry analysis of Western blots (as presented at top, with lanes corresponding to labels of bar graph). Error bars are derived from six repeats of the same experiment. One-way ANOVA detects no significant difference in mean SOS1 expression. (*F*) NMR-derived exchange curves from cell extracts. Lysates normalized for SOS1 expression were assayed for GDP-to-GTPγS exchange activity on ^{15}N-RAS.

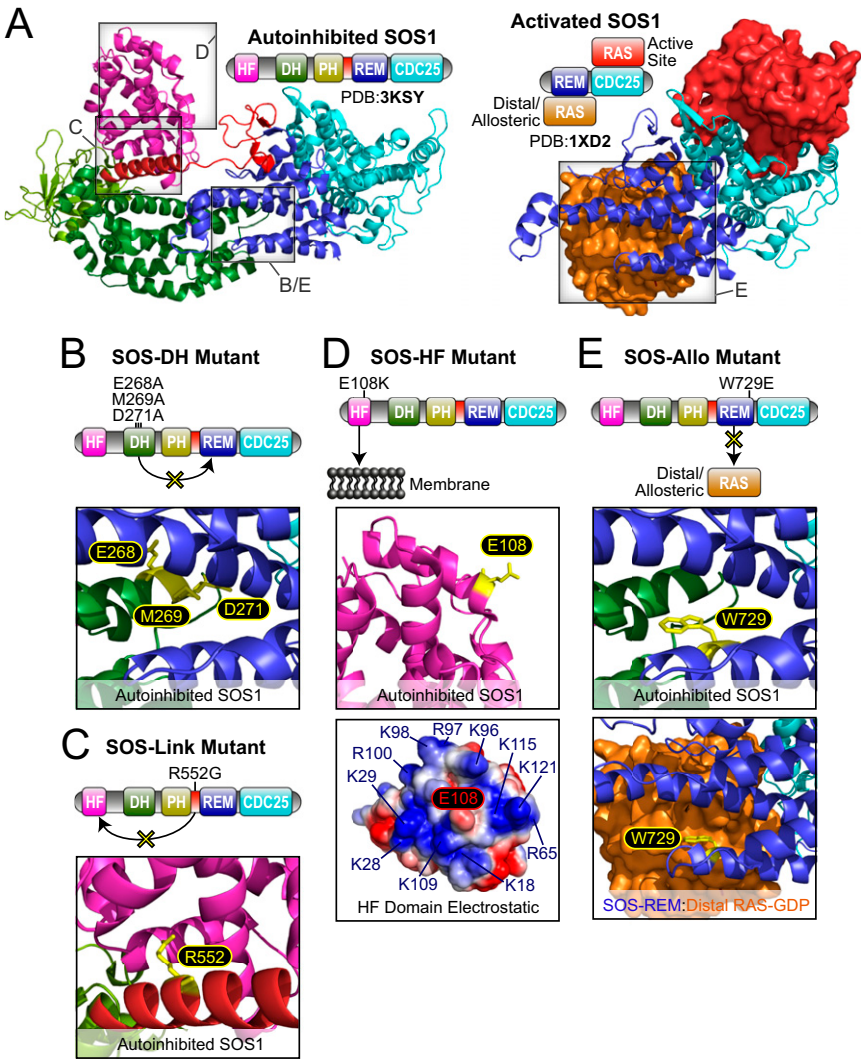

Fig. S4. Structural analysis of SOS1 mutations. (*A*) Crystal structures of autoinhibited SOS^{HDPC} (PDB ID 3KSY) and activated SOS^{cat} (with RAS bound to the active and allosteric sites, PDB ID 1XD2). Outlines of SOS1 modular arrangement are colored by corresponding domain in the depicted structures. Close-ups presented in *B*–*E* are boxed and labeled. RAS proteins are shown as surface representations. (*B*) SOS1 DH domain mutations E286A/M269A/D271A weaken the autoinhibitory regulation provided by DH domain occlusion of the Rem domain allosteric site. Presumably an activating mutant. (*C*) SOS1 linker (SOS1-Link) mutation R552G dislodges the histone fold domain autoinhibitory interaction with the PH-Rem linker. Presumably an activating mutant. (*D*) SOS1 histone fold-domain mutant E108K is thought to increase affinity for lipid membranes. The E108 residue is surface-exposed (*Upper*) and is surrounded by positively charged residues (*Lower*, electrostatic surface representation). Presumably an activating mutant. (*E*) SOS1 allosteric (SOS-Allo) mutant W729E weakens affinity of distal RAS for the Rem domain allosteric site. W729 is at the DH domain interface in the autoinhibited structure (*Upper*) and interacts directly with distal RAS in the activated structure (*Lower*). Presumably a deactivating mutant.

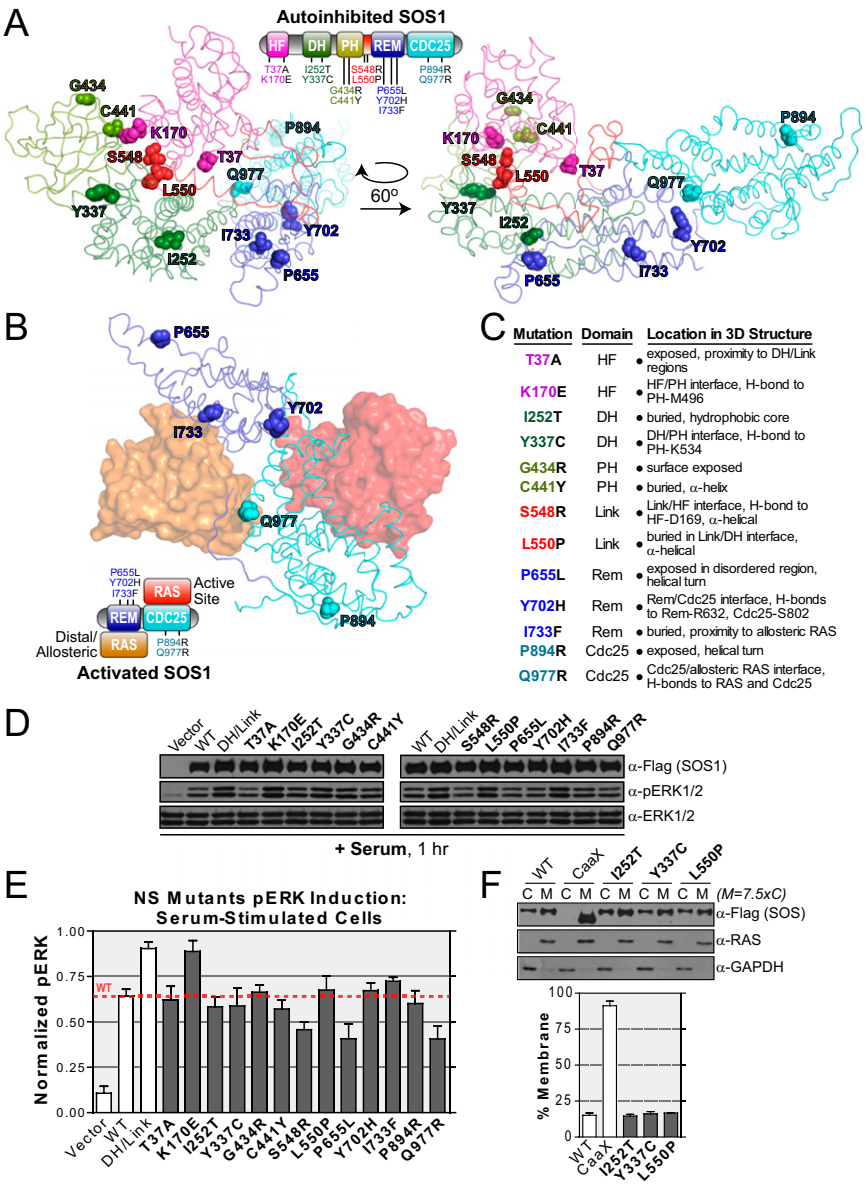

Fig. S5. Structural analysis of NS mutants and their ability to stimulate ERK activation in serum-activated cells. (*A*) Crystal structure of autoinhibited SOS1^{HDPC} (PDB ID 3KSY) is presented in ribbons, colored by corresponding domains in the SOS1 modular outline (*Top*, *Center*). Positions of the 13 NS mutations are marked on the outline, and associated residues highlighted in the ribbons representation. (*B*) Comparable analysis of the five NS mutations located in the SOS1 catalytic region, using the crystal structure of activated SOS^{cat} (PDB ID 1XD2). NS mutations are highlighted in the ribbons representation. RAS proteins are shown as surface representations. (*C*) Chart describes position of the 13 NS mutations, including their localization or proximity to individual SOS1 modular domains and associated hydrogen bonding. (*D*) NS mutants activate the RAS/RAF/MAPK pathway when expressed in cells. SOS1 proteins were Flag-tagged and expressed in HEK 293T cells. Vector alone, SOS-WT and SOS1-DH/Link were included as controls. Western blots showing expressed SOS1 levels (anti-Flag), activated ERK (anti-pERK), and loaded ERK (anti-ERK) are shown for cells that were starved for 24 h and subsequently serum-stimulated for 1 h before lysis. Analogous blots for starved cells are presented in Fig. 5*B*. Results are representative of multiple repeated experiments. (*E*) Quantitation of ERK activation in cells expressing wild-type or NS mutant SOS1 proteins after stimulation with serum for 1 h. Data are derived from densitometry analysis of Western blots from three separate experiments. One-way ANOVA indicates significant differences in mean pERK levels ($P < 0.05$). (*F*) Membrane fractionation of SOS1 variants in starved cells. Immunoblotting with anti-RAS (M, membrane) and anti-GAPDH (C, cytosolic) confirmed fractionation (*Upper*). 7.5-fold membrane fractions were loaded compared with cytosolic. Quantification of SOS1 fractions was performed by densitometry after repeated experiments (*Lower*).

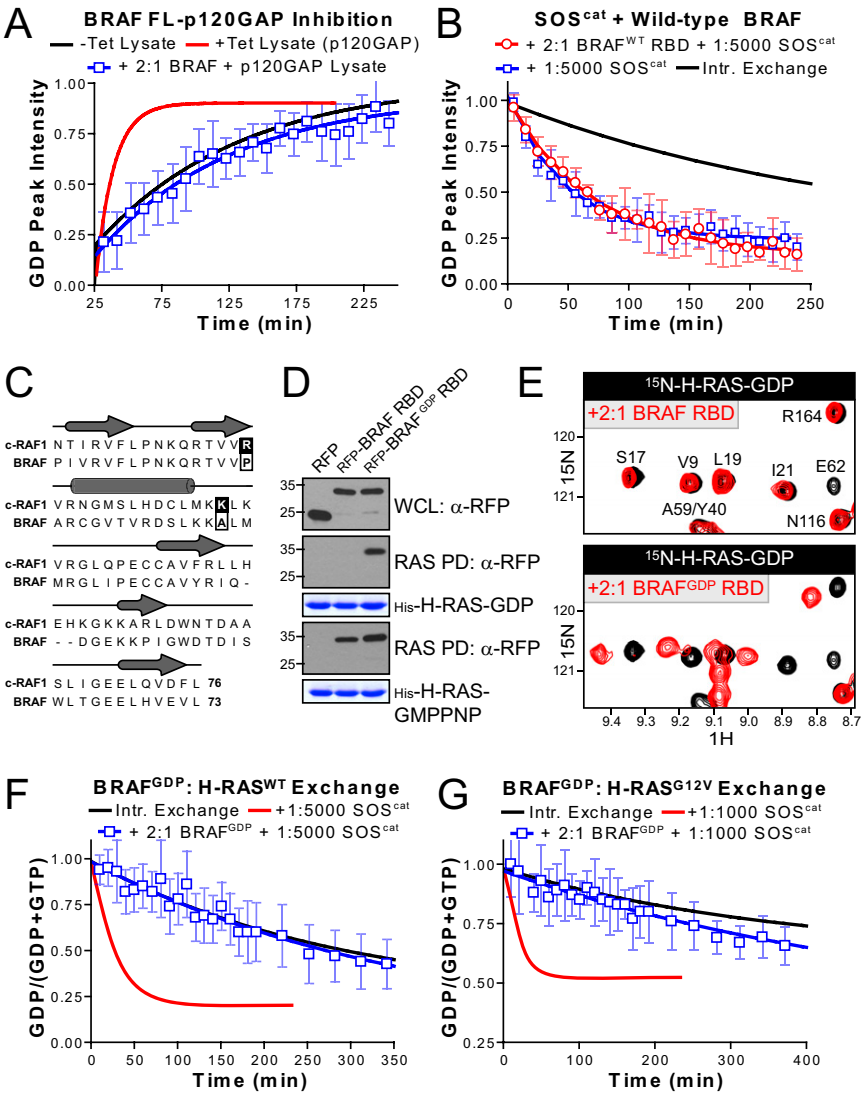

Fig. S6. An effector domain able to bind RAS-GDP inhibits activation. (*A*) Activity of full-length p120GAP is inhibited by BRAF RBD. Tet-induced p120GAP expression stimulates GTP hydrolysis (red line) compared with control lysates (black line), but is completely inhibited by the presence of 2-fold BRAF RBD (box). (*B*) Wild-type BRAF RBD does not significantly inhibit SOS^{cat}-mediated exchange in 10-fold molar excess GTPγS. In the presence of 2-fold molar excess RBD (square), 1:5,000 SOS^{cat} showed an exchange rate comparable to 1:5,000 SOS^{cat} alone (circle). (*C*) Two amino acid substitutions in the BRAF RBD increase its affinity for inactive (GDP-bound) RAS. Alignment of BRAF RBD with c-RAF1 highlighting mutations first identified by Filchtinski et al. (1) (boxed). (*D*) RAS-GDP interacts with $BRAF^{GDP}$ from cells. His-tagged RAS loaded with GMPPNP or GDP was used to pull down RFP-tagged BRAF RBD (wild-type or GDP-binding mutant) expressed in HEK 293T cells. RFP alone was used as control. Expressed proteins are at top (WCL: anti-RFP). RBDs interacting with RAS are shown above RAS loading. (*E*) NMR analysis of $BRAF^{GDP}$. HSQC overlay of select amide resonances from ^{15}N-RAS-GDP alone (black) or in the presence of 2-fold molar excess BRAF RBD (red). Wild-type BRAF shows no significant chemical-shift perturbations (*Upper*), but $BRAF^{GDP}$ demonstrates clear binding (*Lower*). (*F*) SOS^{cat} exchange activity on wild-type RAS is inhibited by $BRAF^{GDP}$. 2-fold molar excess $BRAF^{GDP}$ reduced the typical exchange rate of 1:5,000 SOS^{cat} to near-intrinsic levels. (*G*) $BRAF^{GDP}$ also inhibits oncogenic RAS activation. RAS^{G12V} was assayed for exchange in 10-fold GTPγS, SOS^{cat}, and 2-fold $BRAF^{GDP}$. The mutant RBD obstructed SOS^{cat} exchange activity on G12V to near-intrinsic levels.

1. Filchtinski D, et al. (2010) What makes Ras an efficient molecular switch: A computational, biophysical, and structural study of Ras-GDP interactions with mutants of Raf. *J Mol Biol* 399(3):422–435.

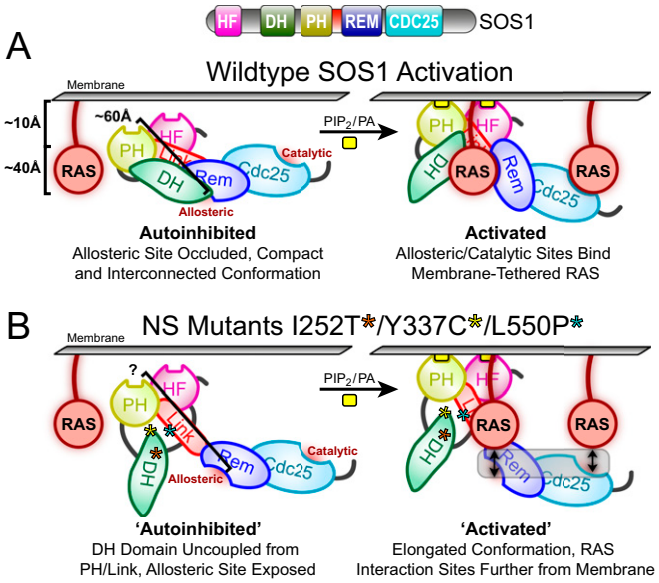

Fig. S7. Model of the mechanism limiting RAS/ERK output in cells from the highly active SOS1 NS mutants I252T, Y337C, and L550P. (*A*) Wild-type SOS1 is autoinhibited by a compact regulatory region consisting of its HF-DH-PH-Linker modules. The DH domain occludes an allosteric RAS binding site in the Rem domain, although interaction between the isolated DH and Rem modules is relatively weak (1). Accordingly, autoinhibition is likely stabilized by an interdomain association network linking the DH domain with the Linker/HF and PH domains. This result is evidenced by data showing a DH-SOS^{cat} construct completely lacks autoinhibition (1). Upon stimulation, lipid modifications result in HF and PH domain membrane binding, whereby SOS1 is placed in close proximity to membrane-tethered RAS. Membrane interactions may also result in a conformational rearrangement in SOS1 that displaces the DH domain and relieves occlusion of the Rem domain allosteric site. These properties activate SOS1 by promoting the RAS-Rem interaction, and subsequently stimulating Cdc25-mediated guanine nucleotide exchange factors (GEF) activity. The maximal distance between RAS and the membrane surface is ~50 Å; thus, the SOS1 allosteric and catalytic sites must be oriented in such a manner that interactions with RAS are sterically achievable within this space. (*B*) The NS mutants I252T, Y337C, and L550P display exceptionally greater exchange activity than wild-type SOS1 (as measured by NMR), but their capacity to induce RAS/ERK signaling in cells is only marginally increased. The membrane binding interfaces and C-terminal Grb2-interaction regions of these mutants remain intact, and they associate with cell membrane and soluble fractions at identical ratios to wild-type (Fig. S5*F*). The NMR assay is dependent on soluble RAS, present in high concentrations and able to orient in any manner required to associate with both the SOS1 allosteric and catalytic sites. The high activity shown by these mutants, and the fit of exchange data to an exponential model, confirm increased RAS access to the allosteric site and demonstrate a loss of membrane-dependent activation. The position of these residues in autoinhibited SOS1 (far removed from both the allosteric and catalytic RAS binding sites) suggests they would uncouple DH domain interactions with the PH domain (Y337C), Linker/HF module (L550P) or destabilize the DH domain itself (I252T). We postulate that loss of the interaction network stabilizing DH domain occlusion of the allosteric site would untether the DH domain and extend the entire N-terminal regulatory region. When bound to membrane this would place the allosteric (and potentially catalytic) site further from the surface, and by extension, from membrane-tethered RAS. Thus, although these NS mutants possess up to 8-fold higher activity than wild-type RAS in solution, the membrane-dependent nature of SOS1-RAS activation in cells moderates this increase, and demonstrates how multilayered SOS1 regulation is able to reduce the impact of three strong gain-of-function mutants.

1. Sacco E, et al. (2012) Regulation of hSos1 activity is a system-level property generated by its multi-domain structure. *Biotechnol Adv* 30(1):154–168.

Table S1. NMR-derived hydrolysis and exchange rates for all experiments in this study

Figure	RAS protein	Reaction	GAP/GEF	Ratio	Nucleotide	Accessory	Ratio	Mean rate	Fold-change
Fig. 1 rates (min^{-1})									
Fig. 1*C*	Wild-type	Hydrolysis	—	—	GTP	—	—	8.8 ± 0.7E-03 min^{-1}	—
	G12V	Hydrolysis	—	—	GTP	—	—	8.9E-04 min^{-1}	10× Below wild-type
	Q61L	Hydrolysis	—	—	GTP	—	—	1.1E-04 min^{-1}	80× Below wild-type
	G13D	Hydrolysis	—	—	GTP	—	—	3.1 ± 0.0E-03 min^{-1}	2.8× Below wild-type
Fig. 1*D*	Wild-type	Exchange	—	—	10× GTPγS	—	—	3.8 ± 0.4E-03 min^{-1}	—
	G12V	Exchange	—	—	10× GTPγS	—	—	2.0 ± 0.6E-03 min^{-1}	1.8× Below wild-type
	Q61L	Exchange	—	—	10× GTPγS	—	—	9.0 ± 0.9E-03 min^{-1}	2.4× Above wild-type
	G13D	Exchange	—	—	10× GTPγS	—	—	56.7 ± 0.7E-03 min^{-1}	15× Above wild-type
Fig. 2/Fig. S2 rates (min^{-1})									
Fig. S2*B*	Wild-type	Hydrolysis	GAP-334	1:5,000	GTP	—	—	54.0 ± 6.6E-03 min^{-1}	6.1× Above intrinsic
	Wild-type	Hydrolysis	GAP-334	1:2,500	GTP	—	—	119.4 ± 10.1E-03 min^{-1}	14× Above intrinsic
	Wild-type	Hydrolysis	GAP-334	1:1,000	GTP	—	—	523.4 ± 57.4E-03 min^{-1}	60× Above intrinsic
Fig. S2*C*	Wild-type	Exchange	SOS^{cat}	1:10,000	10× GTPγS	—	—	12.2 ± 0.3E-03 min^{-1}	3.2× Above intrinsic
	Wild-type	Exchange	SOS^{cat}	1:8,000	10× GTPγS	—	—	17.6 ± 2.0E-03 min^{-1}	4.7× Above intrinsic
	Wild-type	Exchange	SOS^{cat}	1:5,000	10× GTPγS	—	—	25.0 ± 0.4E-03 min^{-1}	6.6× Above intrinsic
Fig. S2*D*	G12V	Hydrolysis	GAP-334	1:2,500	GTP	—	—	No Activity	—
	G12V	Exchange	SOS^{cat}	1:1,000	10× GTPγS	—	—	112.8 ± 32.1E-03 min^{-1}	55× Above intrinsic
Fig. S2*F*	Q61L	Hydrolysis	GAP-334	1:2,500	GTP	—	—	No Activity	—
	Q61L	Hydrolysis	GAP-334	1:1	GTP	—	—	16.3 ± 2.9E-03 min^{-1}	148× Above intrinsic
	Q61L	Exchange	SOS^{cat}	1:5,000	10× GTPγS	—	—	41.9 ± 2.8E-03 min^{-1}	4.6× Above intrinsic
Fig. S2*G*	G13D	Hydrolysis	GAP-334	1:2,500	GTP	—	—	No Activity	—
	G13D	Hydrolysis	GAP-334	1:1	GTP	—	—	27.1 ± 1.1E-03 min^{-1}	9× Above intrinsic
Fig. 3 rates (min^{-1})									
Fig. 3*A*	Wild-type	Hydrolysis	-Tet Lysate	Equal [protein]	GTP	—	—	17.3 ± 0.9E-03 min^{-1}	2.0× Above intrinsic
	Wild-type	Hydrolysis	p120GAP lysate		GTP	—	—	79.6 ± 4.2E-03 min^{-1}	4.6× Above -Tet control
Fig. 3*C*	Wild-type	Hydrolysis	Buffer alone	—	GTP	—	—	8.1 ± 0.0E-03 min^{-1}	—
	Wild-type	Hydrolysis	CRL-2768 lysate	Equal [protein]	GTP	—	—	33.0 ± 0.5E-03 min^{-1}	4.1× Above buffer
	Wild-type	Hydrolysis	CRL-2884 lysate		GTP	—	—	22.0 ± 0.7E-03 min^{-1}	2.7X× Above buffer
Fig. 4/Fig. S3 rates (reported as 1/half-life (min^{-1}) to accurately compare sigmoidal vs. one phase exponential fits									
Fig. 4*A*	Wild-type	Exchange	SOS-WT lysate	3 μL	10× GTPγS	—	—	13.6E-03 min^{-1}	2.9× Above Intrinsic
	Wild-type	Exchange	SOS-WT lysate	14 μL	10× GTPγS	—	—	26.1E-03 min^{-1}	5.5× Above intrinsic
	Wild-type	Exchange	SOS-WT lysate	20 μL	10× GTPγS	—	—	80.8E-03 min^{-1}	17× Above intrinsic
Fig. S3*A*	Wild-type	Exchange	SOS-WT lysate	3 μL	10X GTPγS	RAS-GTPγS	50 μM	16.0 ± 0.2E-03 min^{-1}	1.2× Above SOS-WT
	Wild-type	Exchange	SOS-WT lysate	3 μL	10× GTPγS	RAS-GTPγS	150 μM	18.7 ± 0.2E-03 min^{-1}	1.4× Above SOS-WT
	Wild-type	Exchange	SOS-WT lysate	3 μL	10× GTPγS	G12V-GTP	150 μM	19.0 ± 1.9E-03 min^{-1}	1.4× Above SOS-WT
Fig. S3*B*	Wild-type	Exchange	SOS-WT lysate	3 μL	10× GTPγS	—	—	15.0 ± 1.4E-03 min^{-1}	—
	Wild-type	Exchange	SOS-WT lysate	3 μL	10× GTPγS	RAS-GDP	50 μM	16.2 ± 0.7E-03 min^{-1}	1.1× Above SOS-WT
	Wild-type	Exchange	SOS-WT lysate	3 μL	10× GTPγS	RAS-GDP	150 μM	16.3 ± 0.0E-03 min^{-1}	1.1× Above SOS-WT
Fig. 4*D*/ Fig. S3*F*	Wild-type	Exchange	Vector lysate	Normalized by	10× GTPγS	—	—	4.7 ± 0.2E-03 min^{-1}	Equal to intrinsic
	Wild-type	Exchange	SOS-WT lysate	Western blot/	10× GTPγS	—	—	15.5 ± 0.6E-03 min^{-1}	3.3× Above vector
	Wild-type	Exchange	SOS-HF lysate	densitometry	10× GTPγS	—	—	15.8 ± 2.4E-03 min^{-1}	Equal to wild-type
	Wild-type	Exchange	SOS-DH lysate		10× GTPγS	—	—	25.0 ± 0.6E-03 min^{-1}	1.6× Above SOS-WT
	Wild-type	Exchange	SOS-Link lysate		10× GTPγS	—	—	26.9 ± 0.2E-03 min^{-1}	1.7× Above SOS-WT
	Wild-type	Exchange	SOS-Allo lysate		10× GTPγS	—	—	6.2 ± 0.4E-03 min^{-1}	2.5× Below SOS-WT
	Wild-type	Exchange	SOS-DH/Link lysate		10v GTPγS	—	—	64.0 ± 0.3E-03 min^{-1}	4.1× Above SOS-WT
	Wild-type	Exchange	SOS-δC-CaaX		10× GTPγS	—	—	16.6 ± 1.8E-03 min^{-1}	Equal to wild-type

Table S1. Cont.

Figure	RAS protein	Reaction	GAP/GEF	Ratio	Nucleotide	Accessory	Ratio	Mean rate	Fold-change
Fig. 5 rates (reported as 1/half-life (min^{-1}) to accurately compare sigmoidal vs. one phase exponential fits									
Fig. 5*D*	Wild-type	Exchange	Vector lysate	Normalized by	10× GTPγS	—	—	3.3 ± 0.4E-03 min^{-1}	4.3× Below SOS-WT
	Wild-type	Exchange	SOS-WT lysate	Western blot/	10× GTPγS	—	—	14.3 ± 0.3E-03 min^{-1}	—
	Wild-type	Exchange	SOS-HF lysate	densitometry	10× GTPγS	—	—	62.4 ± 6.3E-03 min^{-1}	4.4× Above SOS-WT
	Wild-type	Exchange	Noonan-T37A		10× GTPγS	—	—	16.2 ± 0.4E-03 min^{-1}	1.1× Above SOS-WT
	Wild-type	Exchange	Noonan-K170E		10× GTPγS	—	—	23.1 ± 0.8E-03 min^{-1}	1.6× Above SOS-WT
	Wild-type	Exchange	Noonan-I252T		10× GTPγS	—	—	39.4 ± 2.4E-03 min^{-1}	2.8× Above SOS-WT
	Wild-type	Exchange	Noonan-Y337C		10× GTPγS	—	—	72.2 ± 8.1E-03 min^{-1}	5.1× Above SOS-WT
	Wild-type	Exchange	Noonan-G434R		10× GTPγS	—	—	21.1 ± 0.9E-03 min^{-1}	1.5× Above SOS-WT
	Wild-type	Exchange	Noonan-C441Y		10× GTPγS	—	—	17.0 ± 1.0E-03 min^{-1}	1.2× Above SOS-WT
	Wild-type	Exchange	Noonan-S548R		10× GTPγS	—	—	22.9 ± 3.0E-03 min^{-1}	1.6× Above SOS-WT
	Wild-type	Exchange	Noonan-L550P		10× GTPγS	—	—	109.7 ± 11.7E-03 min^{-1}	7.7× Above SOS-WT
	Wild-type	Exchange	Noonan-P655L		10× GTPγS	—	—	16.1 ± 1.6E-03 min^{-1}	1.1× Above SOS-WT
Fig. 5*D*	Wild-type	Exchange	Noonan-Y702H	Normalized by	10× GTPγS	—	—	32.9 ± 2.2E-03 min^{-1}	2.3× Above SOS-WT
	Wild-type	Exchange	Noonan-I733F	Western blot/	10X GTPγS	—	—	34.1 ± 2.1E-03 min^{-1}	2.4× Above SOS-WT
	Wild-type	Exchange	Noonan-P894R	densitometry	10X GTPγS	—	—	16.4 ± 1.7E-03 min^{-1}	1.2× Above SOS-WT
	Wild-type	Exchange	Noonan-Q977R		10X GTPγS	—	—	6.6 ± 0.2E-03 min^{-1}	2.1× Below SOS-WT
Fig. 6/Fig. S6 rates (min^{-1})									
Fig. 6*A*	Wild-type	Hydrolysis	—	—	GTP	—	—	8.8 ± 0.6E-03 min^{-1}	—
	Wild-type	Hydrolysis	GAP-334	1:5,000	GTP	—	—	54.0 ± 6.6E-03 min^{-1}	—
	Wild-type	Hydrolysis	GAP-334	1:5,000	GTP	BRAF	2:1	10.1 ± 1.8E-03 min^{-1}	5.3× Below 1:5,000 GAP
Fig. S6*A*	Wild-type	Hydrolysis	-Tet lysate	Equal [Protein]	GTP	—	—	17.3 ± 0.9E-03 min^{-1}	—
	Wild-type	Hydrolysis	p120GAP lysate		GTP	—	—	79.6 ± 4.2E-03 min^{-1}	—
	Wild-type	Hydrolysis	p120GAP lysate		GTP	BRAF	2:1	10.1 ± 2.6E-03 min^{-1}	7.9× Below p120GAP
Fig. S6*B*	Wild-type	Exchange	—	—	10× GTPγS	—	—	3.8 ± 0.4E-03 min^{-1}	—
	Wild-type	Exchange	SOS^{cat}	1:5,000	10× GTPγS	—	—	20.5E-03 min^{-1}	—
	Wild-type	Exchange	SOS^{cat}	1:5,000	10× GTPγS	BRAF	2:1	14.1E-03 min^{-1}	1.4× Below 1:5,000 SOS
Fig. S6*F*	Wild-type	Exchange	SOS^{cat}	1:5,000	10× GTPγS	—	—	25.0 ± 0.4E-03 min^{-1}	—
	Wild-type	Exchange	SOS^{cat}	1:5,000	10× GTPγS	$BRAF^{GDP}$	2:1	2.3 ± 0.4E-03 min^{-1}	11× Below 1:5,000 SOS
Fig. S6*G*	G12V	Exchange	SOS^{cat}	1:1,000	10× GTPγS	—	—	112.8 ± 32.1E-03 min^{-1}	—
	G12V	Exchange	SOS^{cat}	1:1,000	10× GTPγS	$BRAF^{GDP}$	2:1	2.3 ± 0.4E-03 min^{-1}	50× Below 1:1,000 SOS
Fig. 6*B*	Q61L	Exchange	—	—	10× GTPγS	—	—	9.0 ± 0.9E-03 min^{-1}	—
	Q61L	Exchange	—	—	10× GTPγS	$BRAF^{GDP}$	2:1	1.3E-03 min^{-1}	6.7× Below intrinsic
	Q61L	Exchange	SOS^{cat}	1:5,000	10× GTPγS	—	—	41.9 ± 2.8E-03 min^{-1}	—
	Q61L	Exchange	SOS^{cat}	1:5,000	10× GTPγS	$BRAF^{GDP}$	2:1	3.1 ± 0.6E-03 min^{-1}	14× Below 1:5,000 SOS
Fig. 6*D*	Wild-type	Exchange	Vector lysate	25 μL	10× GTPγS	—	—	3.3 ± 0.1E-03 min^{-1}	—
	Wild-type	Exchange	SOS-DH/Link lysate	25 μL	10× GTPγS	—	—	27.6 ± 2.5E-03 min^{-1}	—
	Wild-type	Exchange	SOS-DH/Link lysate	25 μL	10× GTPγS	$BRAF^{GDP}$	2:1	1.5 ± 0.5E-03 min^{-1}	18× Below DH/Link

GAP, GTPase activating protein. Rates are recorded as min^{-1}, and SDs derived from at least two repeats of the same experiment.

Table S2. Nucleotide binding characteristics of H-RAS and oncogenic mutants of H-RAS as compiled from previous literature

RAS protein	nucleotide	Affinity	Dissociation	Association	Method	Conditions
Wild-type (1)	GDP	—	0.79×10^2 (min^{-1})	—	[8-^{3}H]GDP	37 °C, 10 mM $MgCl_2$
G12V (1)	GDP	—	0.23×10^2 (min^{-1})	—	[8-^{3}H]GDP	
Wild-type (1)	GDP	—	0.07×10^2 (min^{-1})	—	[8-^{3}H]GDP	21 °C, 10 mM $MgCl_2$
G12V (1)	GDP	—	0.03×10^2 (min^{-1})	—	[8-^{3}H]GDP	
Wild-type (1)	GDP	—	35×10^2 (min^{-1})	—	[8-^{3}H]GDP	21 °C, 0.1 mM $MgCl_2$
G12V (1)	GDP	—	9×10^2 (min^{-1})	—	[8-^{3}H]GDP	
Wild-type (1)	GTP	—	2.3×10^2 (min^{-1})	—	[γ-^{32}P]GTP	37 °C, 10 mM $MgCl_2$
G12V (1)	GTP	—	0.47×10^2 (min^{-1})	—	[γ-^{32}P]GTP	
Wild-type (1)	GTP	—	17×10^2 (min^{-1})	—	[γ-^{32}P]GTP	21 °C, 0.1 mM $MgCl_2$
G12V (1)	GTP	—	13×10^2 (min^{-1})	—	[γ-^{32}P]GTP	
Wild-type (2)	GDP	—	7.9×10^3 (min^{-1})	—	[γ-^{3}H]GDP	37 °C
G12V (2)	GDP	—	2.3×10^3 (min^{-1})	—	[γ-^{3}H]GDP	
Wild-type (2)	GTP	1.9×	—	—	Relative to GDP, measured	
Wild-type (2)	GTPγS	0.72×	—	—	with [8-^{3}H]GDP	
Wild-type (2)	GMPPNP	0.09×	—	—		
G12V (2)	GTP	0.67×	—	—		
G12V (2)	GTPγS	0.37×	—	—		
G12V (2)	GMPPNP	0.035×	—	—		
Wild-type (3)	GTP	9.4×10^{10} (M^{-1})	8.5×10^{-5} (s^{-1})	8.0×10^{-6} ($M^{-1}s^{-1}$)	—	0 °C, 10 mM $MgCl_2$
Wild-type (3)	GTPγS	2.9×10^{10} (M^{-1})	1.5×10^{-4} (s^{-1})	4.4×10^6 ($M^{-1}s^{-1}$)	—	
Wild-type (4)	GDP	—	—	—	[γ-^{32}P]GDP	—
Q61L (4)	GDP	—	~5× Higher	—	[γ-^{32}P]GDP	—

1. John J, Frech M, Wittinghofer A (1988) Biochemical properties of Ha-ras encoded p21 mutants and mechanism of the autophosphorylation reaction. *J Biol Chem* 263(24):11792–11799.
2. John J, Schlichting I, Schiltz E, Rösch P, Wittinghofer A (1989) C-terminal truncation of p21H preserves crucial kinetic and structural properties. *J Biol Chem* 264(22):13086–13092.
3. Feuerstein J, Goody RS, Webb MR (1989) The mechanism of guanosine nucleotide hydrolysis by p21 c-Ha-ras. The stereochemical course of the GTPase reaction. *J Biol Chem* 264(11): 6188–6190.
4. Feig LA, Cooper GM (1988) Relationship among guanine nucleotide exchange, GTP hydrolysis, and transforming potential of mutated ras proteins. *Mol Cell Biol* 8(6):2472–2478.